Journal of Contaminant Hydrology 209 (2018) 14–23

Contents lists available at ScienceDirect

Journal of Contaminant Hydrology

journal homepage: www.elsevier.com/locate/jconhyd

Infiltration behaviour of elemental mercury DNAPL in fully and partially water saturated porous media

Andrea D'Aniello[a,*], Niels Hartog[b,c], Thomas Sweijen[c], Domenico Pianese[a]

[a] University of Naples Federico II, Department of Civil, Architectural and Environmental Engineering, via Claudio 21, 80125 Napoli, Italy
[b] KWR Watercycle Research Institute, Groningenhaven 7, Nieuwegein, The Netherlands
[c] Utrecht University, Department of Earth Sciences, Environmental Hydrogeology Group, Princetonplein 9, 3584 CC, Utrecht, The Netherlands

ARTICLE INFO

Keywords:
Elemental mercury
DNAPL
PCE
Variably water saturated
Leverett scaling
Scaling parameters

ABSTRACT

Mercury is a contaminant of global concern due to its harmful effects on human health and for the detrimental consequences of its release in the environment. Sources of liquid elemental mercury are usually anthropogenic, such as chlor-alkali plants. To date insight into the infiltration behaviour of liquid elemental mercury in the subsurface is lacking, although this is critical for assessing both characterization and remediation approaches for mercury DNAPL contaminated sites. Therefore, in this study the infiltration behaviour of elemental mercury in fully and partially water saturated systems was investigated using column experiments. The properties affecting the constitutive relations governing the infiltration behaviour of liquid Hg^0, and PCE for comparison, were determined using $P_c(S)$ experiments with different granular porous media (glass beads and sands) for different two- and three-phase configurations. Results showed that, in water saturated porous media, elemental mercury, as PCE, acted as a non-wetting fluid. The required entry head for elemental mercury was higher (from about 5 to 7 times). However, due to the almost tenfold higher density of mercury, the required NAPL entry heads of 6.19 cm and 12.51 cm for mercury to infiltrate were 37.5% to 20.7% lower than for PCE for the same porous media. Although Leverett scaling was able to reproduce the natural tendency of Hg^0 to be more prone than PCE to infiltrate in water saturated porous media, it considerably underestimated Hg^0 infiltration capacity in comparison with the experimental results. In the partially water saturated system, in contrast with PCE, elemental mercury also acted as a nonwetting fluid, therefore having to overcome an entry head to infiltrate. The required Hg^0 entry heads (10.45 and 15.74 cm) were considerably higher (68.9% and 25.8%) than for the water saturated porous systems. Furthermore, in the partially water saturated systems, experiments showed that elemental mercury displaced both air and water, depending on the initial water distribution within the pores. This indicates that the conventional wettability hierarchy, in which the NAPL has an intermediate wetting state between the air and the water phases, is not valid for liquid elemental mercury. Therefore, for future modelling of elemental mercury DNAPL infiltration behaviour in variably water saturated porous media, a different formulation of the governing constitutive relations will be required.

1. Introduction

Mercury is globally recognised for its harmful effects on human health and for the detrimental consequences of its release in the environment (US EPA, 2007a; World Chlorine Council, 2011). Reported symptoms following mercury exposure may include: behavioural changes, tremors, pulmonary toxicity, respiratory failure, hypertension, renal toxicity, skin rashes, and even death (US EPA, 2007b). Mercury can either occur in the environment as a result of natural processes, like volcanic activity, or as a result of anthropogenic activities (Risher, 2003). Typical anthropogenic sources of mercury release in the environment are associated to mercury mining (UNEP, 2002), mercury amalgamation for gold and silver mining (Lechler et al., 2000; UNEP, 2002; Hylander and Meili, 2003), and to industrial activities, such as wood preservation (Bollen et al., 2008), chlor-alkali and thermometer manufacturing plants (Biester et al., 2002; Hylander and Meili, 2003; Bernaus et al., 2006; Arbestain et al., 2009; Brooks and Southworth, 2011; Miller et al., 2013). In particular, liquid elemental mercury (Hg^0) has been observed in the subsurface at chlor-alkali plants worldwide (Scanlon et al., 2005; Deeb et al., 2011; ITRC, 2012; Brooks and Southworth, 2011; Golder Associates, 2011). Once in the subsurface, liquid Hg^0 may be subjected to speciation (Leterme and Jacques, 2013;

* Corresponding author.
E-mail address: andrea.daniello@unina.it (A. D'Aniello).

https://doi.org/10.1016/j.jconhyd.2018.01.001
Received 5 March 2017; Received in revised form 7 December 2017; Accepted 3 January 2018
Available online 08 January 2018
0169-7722/

González-Fernández et al., 2014; Leterme et al., 2014), thus releasing in the water phase organic and inorganic mercury compounds that are more toxic, mobile, and soluble than Hg^0 itself, like dimethylmercury (C_2H_6Hg), or to volatilization, in the unsaturated zone, of gaseous mercury (Walvoord et al., 2008), due to its high vapour pressure, 0.07 Pa (CRC, 2014). Due to the low aqueous solubility of elemental mercury of 0.07 mg/l (Eichholz et al., 1988), it can act as a source of mercury contamination in soil and groundwater systems for decades (Davis et al., 1997).

Combined with its high density, of about 13.5 kg/l, (CRC, 2014), liquid elemental mercury behaves like an immiscible Dense NonAqueous Phase Liquid (DNAPL) in the subsurface, although its physical properties strongly differ from more widely studied DNAPLs, such as creosote, carbon tetrachloride, trichloroethylene (TCE) and tetrachloroethylene (PCE), (Schwille, 1988; Busby et al., 1995; Hofstee et al., 1998a; Hofstee et al., 1998b; Oostrom et al., 1999; Wu et al., 2000; Oostrom et al., 2003). For example, elemental mercury has an 8 times higher density, an almost 2 times higher viscosity, and an approximately 15 times higher surface tension than PCE (Schwille, 1988; CRC, 2014).

Insight into the infiltration and flow behaviour of elemental mercury in the subsurface is critical for effective characterization and remediation approaches. Although in petroleum engineering liquid elemental mercury is extensively used as a nonwetting fluid for the analysis of the pore structure (mercury porosimetry) of geological formations under vacuum conditions (Wardlaw and Taylor, 1976; Vavra et al., 1992; Pittman, 1992; Smith et al., 2002; Newsham et al., 2004; Ruth et al., 2013), only recently a few studies (Devasena and Nambi, 2010; Sweijen et al., 2014; D'Aniello, 2017; D'Aniello et al., 2018) have addressed liquid Hg^0 infiltration behaviour in water saturated porous media under environmental conditions. Devasena and Nambi (2010) confirmed that liquid Hg^0 acts as a nonwetting fluid, thus requiring to overcome an entry head to infiltrate into water saturated granular porous media, and that residual mercury entrapment in the two-phase Hg^0-water system was much lower (0.04) than in the TCE-water (0.14) and PCE-water (0.17) systems. They argued that this significant variation in residual saturation was probably due to the high interfacial tension of mercury with water, and to its high density and viscosity, and that mercury DNAPL flow behaviour is governed by gravitational and capillary forces, and is practically independent of viscous forces. Supported by field site characterization of mercury DNAPL distribution, Sweijen et al. (2014) made a first attempt for the modelling of the infiltration and distribution behaviour of elemental mercury in a sandy aquifer for water saturated conditions. In particular, the numerical comparison between Hg^0 and PCE DNAPLs infiltration behaviour indicated that Hg^0 had a higher potential to penetrate to greater depths than PCE, a difference which was further enhanced in the presence of horizontally layered heterogeneities.

Although these studies have shed light on the behaviour of liquid elemental mercury once it has reached the saturated zone, to date, however, it is unclear how this behaviour compares with that in partially water saturated conditions. Moreover, the validity of the classical constitutive relations (Parker et al., 1987), used to describe DNAPLs flow behaviour, as well as the scaling theory (Lenhard and Parker, 1987), is uncertain for liquid elemental mercury in both fully and partially water saturated systems.

To address these knowledge gaps, this study aimed to evaluate the infiltration behaviour of elemental mercury in both fully and partially water saturated conditions for a range of ideal (glass beads) and natural (sands) porous media. The constitutive relations governing Hg^0 DNAPL infiltration behaviour were evaluated using capillary pressure-saturation, $P_c(S)$, experiments performed on these porous media.

Table 1
Porous media physical properties.

Porous medium	ρ_s (g/cm^3)	d_{50} (mm)	Size range (mm)
Coarse Glass Beads[a]	2.65	1	Uniform Distribution
Medium Glass Beads[b]	2.65	0.375	0.200–0.500
Fine Glass Beads[b]	2.65	0.175	0.100–0.250
Medium Sand 1[c]	2.67	0.39	0.200–0.500
Medium Sand 2[c]	2.65	0.26	0.125–0.355

[a] Glaswarenfabrik Karl Hecht (2013).
[b] Retsch (2013).
[c] FILCOM (2015). Particle size classification based on Wentworth classification (1922).

2. Materials and methods

2.1. Porous media

Three types of glass beads, *coarse* (d_{50} = 1 mm), *medium* (d_{50} = 0.375 mm), and *fine* (d_{50} = 0.175 mm), (Glaswarenfabrik Karl Hecht; Retsch), and two different medium sands, Filtersand 0.2–0.5 mm and Silversand S60 (FILCOM-Sibelco Group), were used as porous media (Table 1). The two medium sands will be referred to as *medium sand 1* (MS1) and *medium sand 2* (MS2). The particle size distribution of MS1 (d_{50} = 0.39 mm) is wider (Fig. 1; Table 1) than MS2 (d_{50} = 0.26 mm), and the particle sizes mainly fall in the range of 0.200–0.500 mm and 0.125–0.355 mm, for MS1 and MS2, respectively. For each granular porous medium, information regarding hydraulic conductivity and intrinsic permeability were obtained experimentally using the falling head method (Bear, 1972).

2.2. Fluids

Demineralized water was used as the wetting fluid, while laboratory grade (≥ 99%) tetrachloroethylene (PCE), (Acros Organics), and 99.9 + % redistilled liquid elemental mercury (Hg^0), (Alfa Aesar), were used as the nonwetting fluids for the $P_c(S)$ measurements (Table 2).

2.3. Columns

Column experiments were performed to determine the intrinsic permeability and the $P_c(S)$ curves for different two- and three-phase systems under stable flow conditions. Two cylindrical columns with identical dimensions (42 mm diameter by 51 mm length) were used. One column was made of Poly-Methyl Methacrylate (PMMA) and was used for all the experiments except those involving PCE, as it is wetting with respect to PMMA. Hence, to prevent preferential flow along the column wall, a stainless steel column was used. The two columns were

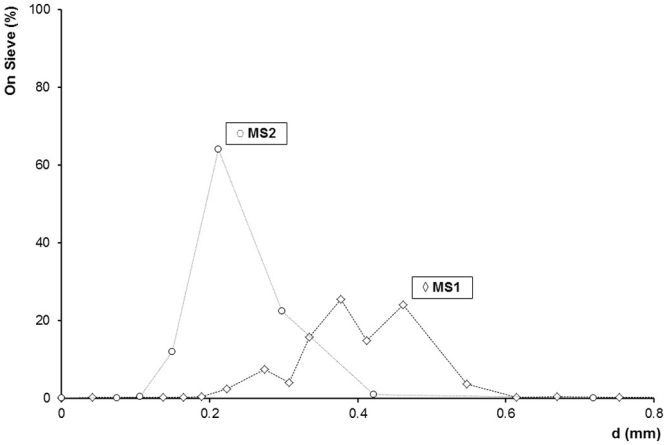

Fig. 1. Particle size frequencies of the medium sand samples (MS1 and MS2). Data from FILCOM (2015).

Table 2
Fluids properties.

Parameter	Unit	Hg^0	PCE	Water
Density	g/cm^3	13.5[a]	1.63[b]	0.998
Dynamic Viscosity	10^{-3} Pa·s	1.55[c] (at 20 °C)	0.89[b] (at 20 °C)	0.98
Surface Tension	Dynes/cm	485[d]	32.6[e]	72
Interfacial Tension with Water	Dynes/cm	375[c]-415[d]	47.8[b]	–
Vapour Pressure	Pa	0.07[a] (at 10 °C)	1867[a] (at 20 °C)	–
Aqueous Solubility	mg/l	0.06–0.08[a]	225[f]	–

[a] CRC (2014).
[b] Pennell et al. (1996).
[c] US DOE (2001) and references therein.
[d] Adamson and Gast (1997).
[e] Mercer and Cohen (1990).
[f] Imhoff et al. (1995).

closed by two caps, each of them provided with a rubber ring to ensure water and air tightness.

The packing of the porous media was performed under water saturated conditions to avoid any presence of entrapped air within the grains. The column was initially filled halfway with water and then, after having thoroughly mixed the grains with water in another container, the solid particles were gradually poured into it. In order to maintain a fully water saturated system, attention was paid to constantly ensure a water head over the top layer of the porous medium. At each filling step, each layer was subjected to the same degree of tamping. A nylon filter, with coarse mesh size, was put at the inflow and outflow ports of the column to prevent loss of solid particles. This filter acted as a water wet membrane, and had a sufficiently coarse mesh size to not affect the measurements. At the end of the packing procedure, the porosity was analytically derived based on the volume and the weight of the filled column, and the densities of both water and the solid particles.

2.4. Capillary pressure-saturation measurements

After filling the columns with the porous media, these were used to determine the $P_c(S)$ retention curves (Fig. 2).

Glass burettes were used to host the wetting and the nonwetting fluids, and both top ports of the burettes were covered with an aluminium foil cap, to prevent any liquid loss through volatilization. The columns and the burettes were connected by Tygon tubes, while, for the PCE experiments, they were connected using a combination of Viton and Teflon tubes. Bottom and top valves of the columns had a three way configuration, which allowed the removal of any entrapped air in the tubes connecting the columns to the glass burettes. Valves were made of Polystyrene (PS), exception for the bottom valve used for the PCE experiments, where stainless steel was used. The choice of different materials for valves and connections was dictated by: i) the incompatibility of PS and Tygon to PCE, and ii) by the tendency of elemental mercury to adsorb to metallic surfaces, such as stainless steel components.

In the Air-Water experiments, the column was connected at the bottom to a burette filled with water, while the top of the column was left in contact with air and covered with an aluminium foil cap to prevent water loss through evaporation. In the two-phase NAPL-Water experiments, the columns were connected at the top to a burette filled with water, while, at the bottom, to a burette filled with NAPL. An additional nylon filter (10 μm mesh size, of about 0.1 mm thickness) was inserted all around the column port, mechanically sealed with the port junction, and placed on the top of the porous sample as a water wet membrane, to allow the flow of water and not of the NAPL. The NAPL was passed from below in order to maintain a stable interface with water, thus avoiding the triggering of gravity induced instability phenomena, such as fingering (Mayer and Hassanizadeh, 2005).

In the Hg^0-Air-Water experiments, the top of the column was connected to an empty burette, in contact with air. These three-phase retention curves were determined after having obtained, for each sample, the drainage branch of the retention curve for the Air-Water system. Hence, the sample structure (porosity and intrinsic permeability) was the same between the two couples of experiments. Within each sample, the air phase was continuous, thus giving the possibility to determine whether Hg^0 was able to infiltrate into a partially water saturated porous medium or not, and, in particular, to evaluate the head required to overcome the resistance exerted by the presence of air within the pores.

The drainage branch of the retention curves was explored by subjecting the columns to stepwise increments in capillary head. In the Air-

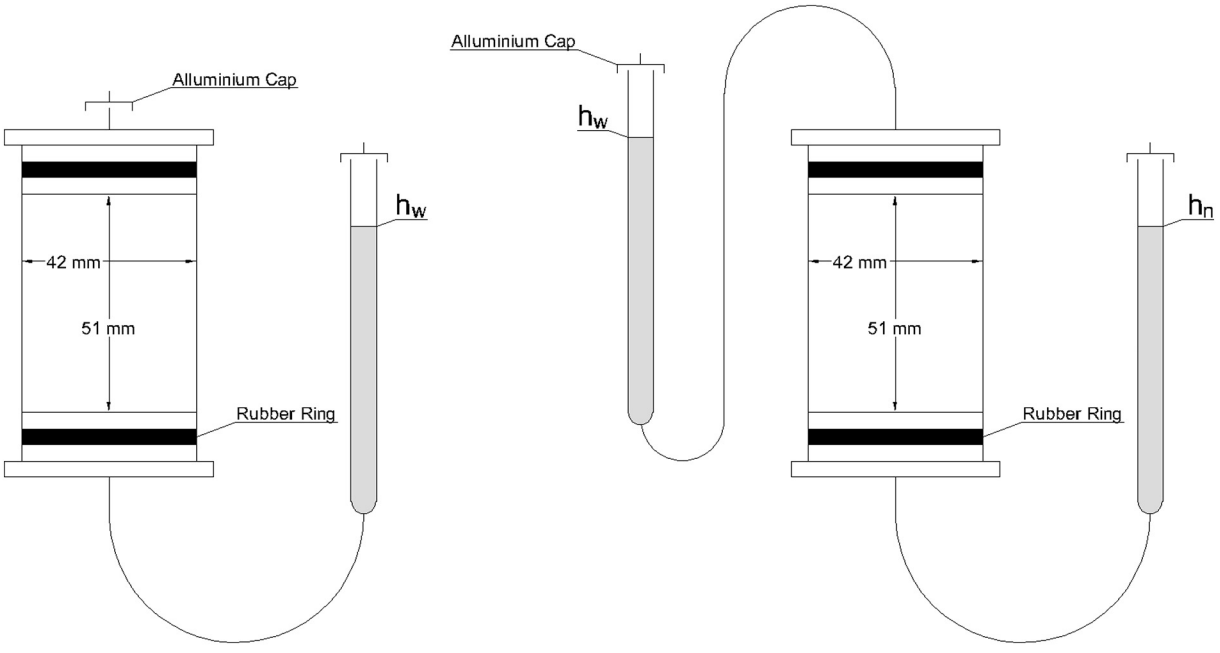

Fig. 2. Air-Water (left) and NAPL-Water (right) $P_c(S)$ setups.

Water experiments, this was achieved by gradually lowering the water filled burette, whereas, in the other experiments, by gradually elevating the NAPL filled burette. At each step, the levels in the burettes were allowed to equilibrate until no further changes were observed. At each step, the water saturation was calculated based on the initial water volume in the sample and the volume increments in the water filled burette. Only in the Hg^0-Air-Water experiments, the Hg^0 saturation was calculated at each step based on the volume decrements in the Hg^0 filled burette. In the Air-Water experiments, the stepwise procedure was continued until the water in the bottom tube became disconnected due to the presence of air, symptom that the air phase became continuous from the top to the bottom of the sample. In the other experiments, the procedure was continued until the breakthrough of NAPL from the top of the columns.

The experimental determinations were fitted by means of SWRC fit (Seki, 2007), adopting the van Genuchten-Mualem model (Mualem, 1976; van Genuchten, 1980):

$$S = S_{w,ir} + (1 - S_{w,ir})\cdot\overline{S} \quad (1)$$

$$\overline{S} = [1 + (\alpha h_c)^n]^{-m} \quad (2)$$

where S is the wetting phase saturation, $S_{w,ir}$ is the irreducible water saturation, $\overline{S}$ is the effective wetting phase saturation, h_c is the capillary head between nonwetting and wetting phases, α, n and m are the van Genuchten model parameters, with m equal to 1–1/n (n > 1). Since the data revealed an incremental rather than a stepwise infiltration pattern at entry head (Section 3.2; Figs. 3–9), the van Genuchten-Mualem model was chosen, as it gives the best fit of the initial branch of the drainage curves. The parameters taken into account in the fitting procedure were α and n, whereas the irreducible water saturation was assumed to be zero due to the lack of measured data in the last branch of the $P_c(S)$ curves. To study the effects of this assumption, the $P_c(S)$ data were fitted again assuming the values of 0.05 and 0.10 for the irreducible water saturation. As a result, there was no substantial change in the van Genuchten fit of the α parameter with respect to the values obtained with $S_{w,ir} = 0$, with variations ranging from the 0.23% to the 1.41% for $S_{w,ir} = 0.05$, and from the 0.48% to the 2.88% for $S_{w,ir} = 0.10$. Moreover, this assumption had no effect on the estimation of the nonwetting phase entry heads, since these were determined with the graphical method (Sillers et al., 2001; Pasha et al., 2015), based on the raw data (Appendix, Fig. A.1).

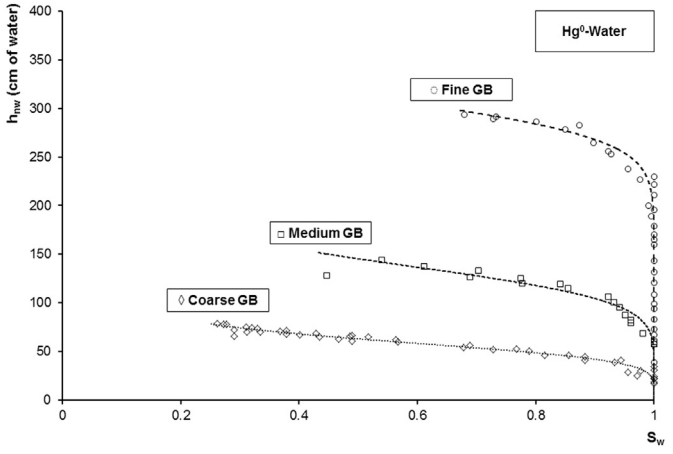

Fig. 3. Observed (symbols) and fitted (dashed lines) Hg^0–Water $P_c(S)$ curves (Glass Beads).

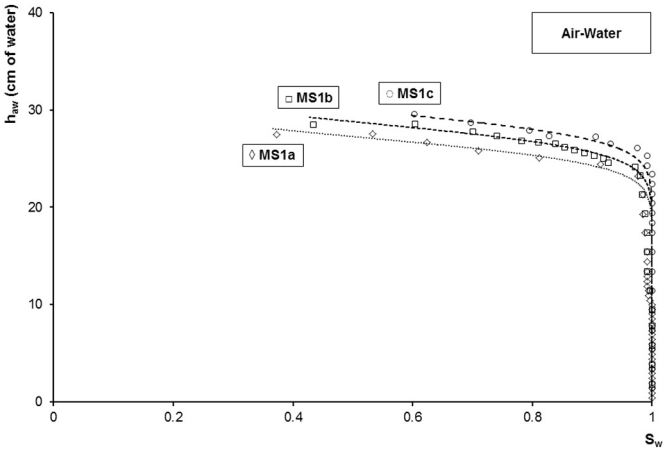

Fig. 4. Observed (symbols) and fitted (dashed lines) Air–Water $P_c(S)$ curves (MS1).

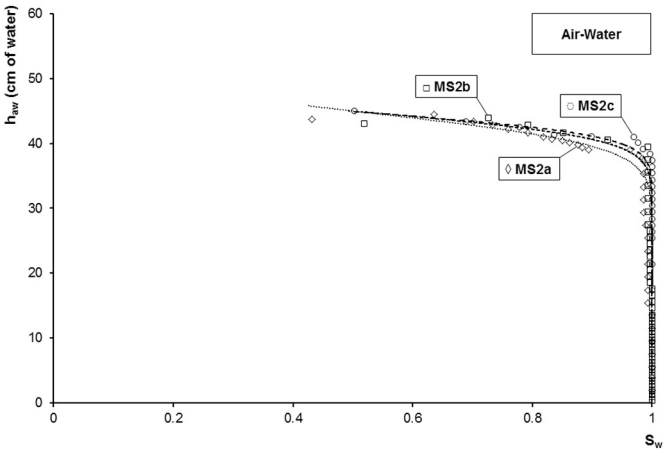

Fig. 5. Observed (symbols) and fitted (dashed lines) Air–Water $P_c(S)$ curves (MS2).

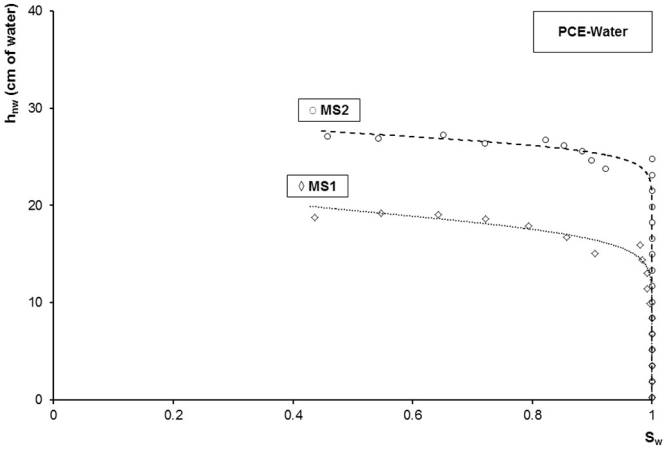

Fig. 6. Observed (symbols) and fitted (dashed lines) PCE–Water $P_c(S)$ curves (MS1 and MS2).

3. Results

3.1. Hydraulic conductivity measurements

Results showed that the intrinsic permeability (Table 3) of the glass beads decreased with decreasing particle size, with small variation in porosity. For the medium sands, both porosity and intrinsic permeability of MS1 were slightly lower than MS2.

Although based on the particle size range (Table 1) alone MS1

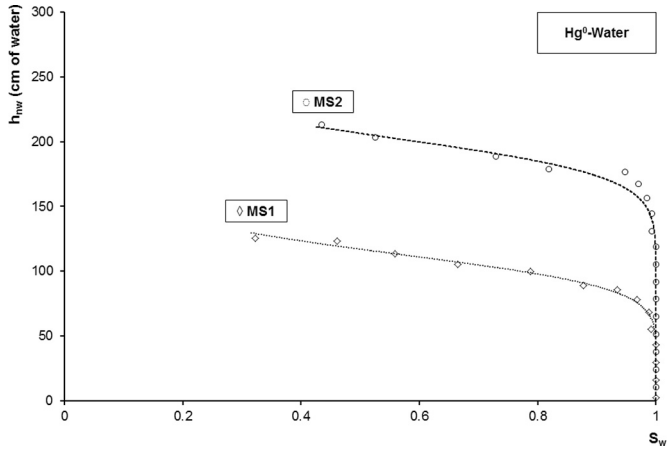

Fig. 7. Observed (symbols) and fitted (dashed lines) Hg^0–Water $P_c(S)$ curves (MS1 and MS2).

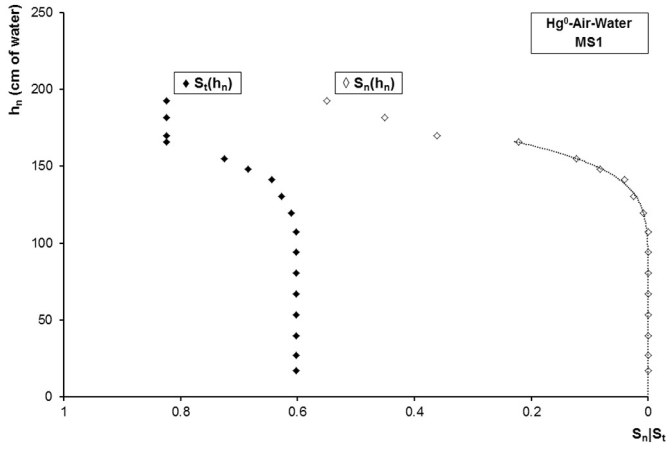

Fig. 8. Observed (symbols) and fitted (dashed lines) Hg^0–Air–Water $P_c(S)$ curves (MS1).

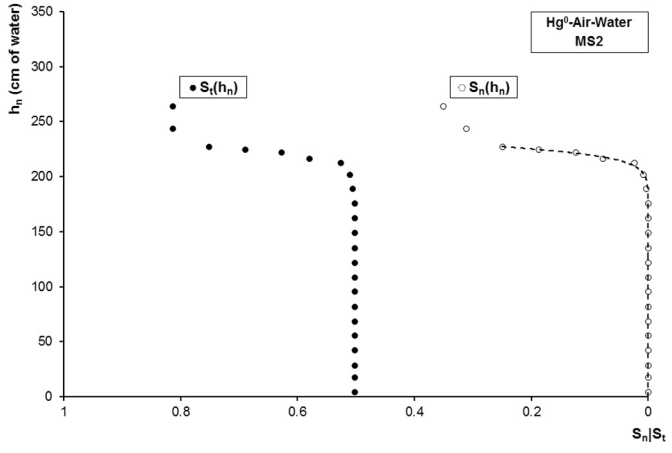

Fig. 9. Observed (symbols) and fitted (dashed lines) Hg^0–Air–Water $P_c(S)$ curves (MS2).

would be expected to have a higher intrinsic permeability than MS2, it also has a wider particle size distribution (Fig. 1), which negatively affects its intrinsic permeability. As a consequence, the resulting intrinsic permeability of MS1 and MS2 is similar.

3.2. Capillary pressure-saturation curves

The $P_c(S)$ curves were obtained for Hg^0-Water in the three types of glass beads (Fig. 3), and for MS1 and MS2 for Air-Water (samples MS1a-b-c and MS2a-b-c; Figs. 4 and 5), PCE-Water (samples MS1d and MS2d; Fig. 6), Hg^0-Water (samples MS1e and MS2e; Fig. 7), and Hg^0-Air-Water (samples MS1c_bis and MS2c_bis; Figs. 8 and 9).

Table 3
Determined porosity and intrinsic permeability of the porous media used.

Porous medium	ϕ	k_{mean} [a] (10^{-7} cm^2)	k_{min} – k_{max} (10^{-7} cm^2)
Coarse Glass Beads	0.410	45.15	44.76–46.14
Medium Glass Beads	0.440	9.43	9.30–9.59
Fine Glass Beads	0.440	1.91	1.86–2.01
Medium Sand 1	0.368	1.61	1.53–1.67
Medium Sand 2	0.391	1.79	1.78–1.80

[a] Number of measurements = 4.

In Figs. 8 and 9, the Hg^0 head (h_n) is plotted versus the nonwetting Hg^0 saturation (S_n) and the total liquid saturation (S_t) for MS1 and MS2, respectively. In contrast with other DNAPLs, elemental mercury had to overcome an entry head to infiltrate and migrate into the partially water saturated samples. As elemental mercury infiltrated, S_n increased, and, at a certain point, the rise in the Hg^0 head no longer induced any increase in the total liquid saturation. At this point, the infiltration of mercury resulted in the expulsion of an equal volume of water from the top of the sand column, and in the entrapment of discontinuous air of about the 20% of the pore volume.

On the basis of the experimental observations previously shown, in partially water saturated porous media, the Hg^0 infiltration is also affected by the presence of water in the pores. Once mercury overcomes the resistance exerted by continuous air and infiltrates within the sample, it also displaces water. Prior to Hg^0 infiltration, the air phase is expected to be present in higher saturations in bigger pores, hence, as elemental mercury infiltrates, it is likely to find a preferential pathway through smaller pores, mostly filled with water. Even though the pores are smaller, elemental mercury displaces the water phase easier than air, due to the lower interfacial tension with water (Table 2). To further enforce this, the comparison of the entry heads required by mercury to infiltrate in fully and partially water saturated sands (Table 4) clearly shows that Hg^0 entry heads considerably increase in presence of air. As mercury infiltration continues, the air phase becomes discontinuous and entrapped within both liquid phases, and most of the elemental mercury comes in contact with water. At this point, a further infiltration of mercury induces the displacement of an equal amount of water, as shown in the last branch of the $P_c(S_t)$ curves in Figs. 8 and 9, until the breakthrough of Hg^0 in the outflow port of the column.

The results obtained from the $P_c(S)$ experiments for each two- and three phase system are summarized in Table 4.

In Table 4, $S_{w,0}$ is the initial water saturation of the porous sample, while h_e denotes the entry head required by the nonwetting phase to infiltrate into the granular porous medium.

4. Discussion

Based on the results, the infiltration behaviour of Hg^0 in granular porous media is analysed and discussed. First, the results of the two- and three-phase $P_c(S)$ experiments are discussed in relation to the samples intrinsic permeability and porosity to assess the role played by porous media characteristics on Hg^0 infiltration behaviour. Then, the infiltration behaviour of elemental mercury in water saturated systems is compared with that of PCE, aiming to verify the applicability of the traditional scaling theory separately for each sand type. The Hg^0 infiltration behaviour and the scaling of its retention properties in variably water saturated systems are finally addressed.

4.1. Hg^0 infiltration behaviour and porous media characteristics

Pore structure is a key aspect that affects the infiltration behaviour

Table 4
$P_c(S)$ Experiments - results.

Sample	System	ϕ	$S_{w,0}$	α (cm^{-1})	n	h_e (cm of water)	h_e (cm of NAPL)
Coarse GB[a]	Hg^0-Water	0.410	1	0.0167	5.58	38.40	2.84
Medium GB[a]	Hg^0-Water	0.440	1	0.0071	6.83	113.03	8.36
Fine GB[a]	Hg^0-Water	0.440	1	0.0032	14.04	262.71	19.42
MS1a	Air-Water	0.365	1	0.0368	19.17	24.02	–
MS1b	Air-Water	0.363	1	0.0349	19.04	25.13	–
MS1c	Air-Water	0.359	1	0.0334	19.95	26.10	–
MS2a	Air-Water	0.385	1	0.0223	17.17	39.58	–
MS2b	Air-Water	0.383	1	0.0223	21.58	40.04	–
MS2c	Air-Water	0.373	1	0.0223	24.95	40.32	–
MS1d	PCE-Water	0.353	1	0.0517	13.41	16.17	9.90
MS2d	PCE-Water	0.375	1	0.0365	28.99	25.75	15.77
MS1e	Hg^0-Water	0.354	1	0.0087	7.97	83.69	6.19
MS2e	Hg^0-Water	0.375	1	0.0049	12.83	169.19	12.51
MS1c_bis	Hg^0-Air-Water	0.359	0.602	0.0054	10.85	141.33	10.45
MS2c_bis	Hg^0-Air-Water	0.373	0.502	0.0043	32.62	212.90	15.74

[a] GB - Glass Beads.

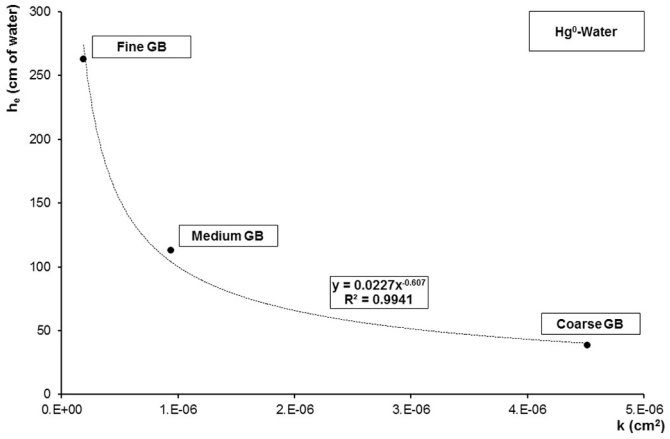

Fig. 10. Nonwetting phase entry head (h_e) versus intrinsic permeability (k) in glass beads (Hg^0-Water).

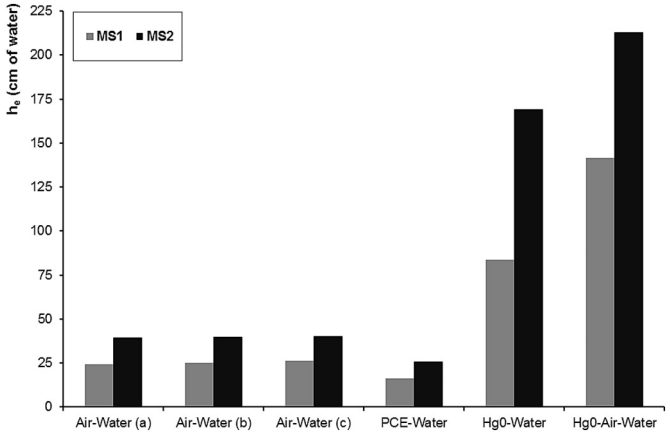

Fig. 11. Nonwetting phase entry heads (h_e) for MS1 and MS2 (all fluid systems).

of elemental mercury, as illustrated by the correlation of entry head with intrinsic permeability (Fig. 10) found in the two-phase glass beads systems analysed. A power law results in the best fit of the data, thus showing a general tendency of the entry head to be higher in samples with lower intrinsic permeability, but not necessarily with lower porosity (Tables. 3 and 4). Although intrinsic permeability is a bulk parameter affected by the combined inner pore structure characteristics of a porous medium, it related with the more locally expressed entry head for the glass beads samples. However, within the small range in intrinsic permeability of the medium sand samples used, the correlation did not hold. Despite the somewhat (11%) higher intrinsic permeability of MS2 (Table 3), the entry head is higher than for MS1 (Fig. 11). Likely, this is the result of the smaller particle size and narrow range in MS2 than MS1 (Fig. 1), which limit the potential for locally present larger pores.

4.2. Leverett scaling in PCE-water and Hg^0-water systems

As the fluid properties of PCE and elemental mercury strongly differ (Table 2), their infiltration behaviour is expected to differ as well. The α parameter, typically used for scaling purposes in numerical modelling (Parker et al., 1987), for elemental mercury is lower than for PCE (Table 4) and, conversely, the entry heads are higher if expressed in terms of water head. However, in terms of the respective DNAPL heads, PCE requires to overcome an entry head of about 60% higher than Hg^0 for MS1, while of about 26% for MS2. This is considerably more than when assuming Leverett scaling (Leverett, 1941) to be applicable (Devasena and Nambi, 2010). Neglecting the effect of the contact angle, a general form of the Leverett function (J), at a given water saturation (S_w), is given by (Leverett, 1941):

$$J(S_w) = \frac{P_c}{\sigma} \bullet \sqrt{\frac{k}{\phi}} \tag{3}$$

where P_c is the capillary pressure, σ is the fluid pair interfacial tension, k is intrinsic permeability, and ϕ is porosity. Since the $J(S_w)$ function is a constant at a given water saturation (Demond and Roberts, 1991), Eq. 3 can be used to scale capillary pressures between different fluid systems. Therefore, after simple manipulations of Eq. 3, the relation between Hg^0 and PCE entry heads (h_e) can be defined as follows, under the hypothesis of no flow, hydrostatic pressure distribution, and assuming the pore structure to be identical for the two systems (as for each sand type the couples of samples studied have practically the same porosity, Table 4):

$$h_e^{Hg} = h_e^{PCE} \bullet \left(\rho_{PCE} / \rho_{Hg} \right) \bullet \left(\sigma_{Hg-W} / \sigma_{PCE-W} \right) \tag{4}$$

where ρ denotes the fluid density.

Using the fluids properties reported in Table 2, Eq. 4 yields that $h_e^{Hg} = 0.947 \cdot h_e^{PCE}$ and $h_e^{Hg} = 1.048 \cdot h_e^{PCE}$, with $\sigma_{Hg\text{-}w}$ equal to 375 dyn/cm and 415 dyn/cm, respectively. Hence, according to Leverett scaling, in the first case, PCE should require to overcome an entry head of about 5.6% higher than Hg^0 to infiltrate in the same porous medium, while, in the latter, PCE entry head would be of about 4.6% lower than Hg^0. Whereas in the first case Leverett scaling is able to reproduce the natural tendency of Hg^0 to be more prone than PCE to

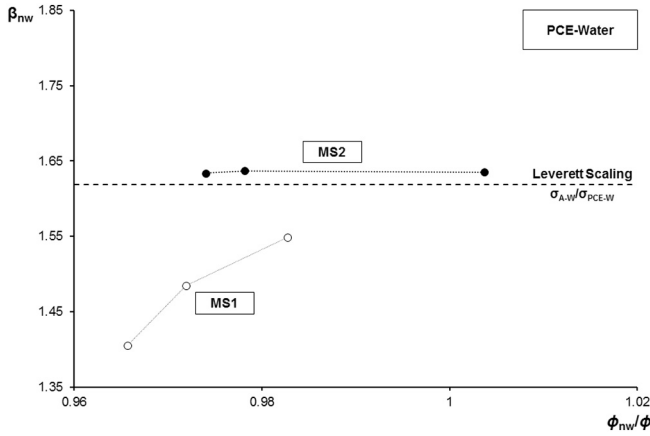

Fig. 12. Experimental PCE-Water scaling parameters (β_{nw}) versus samples porosity ratio (ϕ_{nw}/ϕ_{aw}).

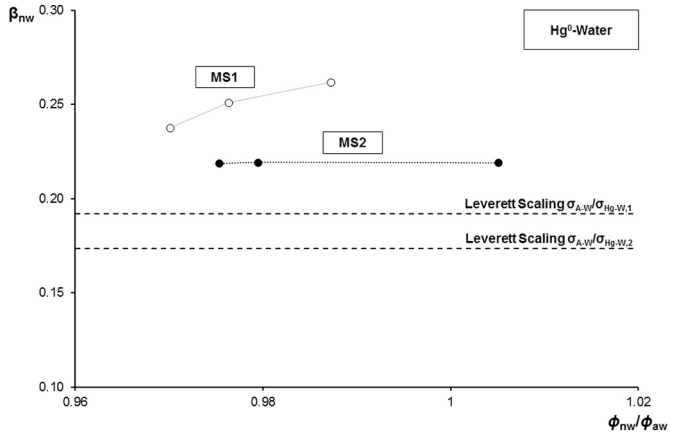

Fig. 13. Experimental Hg^0-Water scaling parameters (β_{nw}) versus samples porosity ratio (ϕ_{nw}/ϕ_{aw}).

infiltrate in water saturated porous media, although it considerably underestimates Hg^0 infiltration capacity in comparison with the experimental results, in the latter case Leverett scaling fails, showing an opposite behaviour than the experimental evidence.

4.3. Experimental scaling parameters for PCE-water and Hg^0-water systems

In Fig. 12, the observed PCE-Water scaling parameters (β_{nw}), defined as the ratio (α_{nw}/α_{aw}) between the DNAPL-Water and the three Air-Water α parameters (Lenhard and Parker, 1987), are plotted versus the samples porosity ratio (ϕ_{nw}/ϕ_{aw}), the ratio between the DNAPL-Water and the three Air-Water samples porosity, for MS1 and MS2, respectively. To verify the ability of the scaling theory to cope with PCE behaviour, the Leverett scaling parameter, given as the ratio between the water surface tension ($\sigma_{A\text{-}W}$) and the DNAPL interfacial tension with water ($\sigma_{PCE\text{-}W}$), Table 2, (Lenhard and Parker, 1987), calculated taking into account the non-spreading behaviour of PCE (White et al., 2004), is also plotted.

For MS1, the observed scaling parameters get closer to the value based on the fluid properties (1.618), with underestimations ranging from 15% to 4.5% as the porosity ratio approaches unity, and the pore structure likely becomes more similar between the couples of samples analysed. For MS2, instead, the agreement between the experimental determinations and the Leverett scaled value is definitely good, with only a slight overestimation of about 1%. These results show that the scaling procedure is applicable for the two-phase PCE-Water system, congruently with the experimental evidence found in sands for other NAPLs, like benzene, p-cymene, o-xylene, and benzyl alcohol (Lenhard and Parker, 1987), and Soltrol 170®, toluene, and TCE (Busby et al., 1995). In particular, for these studies, the reported deviations between Leverett and experimental scaling parameters are 12%, 5.2%, 5.8%, 5%, 1.8%, 15%, and 5%, respectively.

The agreement found for PCE between Leverett and experimental scaling parameters was less for elemental mercury (Fig. 13).

For MS2, the differences between the experimentally determined values are negligible, and the deviations from the values based on the fluids properties (0.192 and 0.173), given as the ratio between the water surface tension and the Hg^0 interfacial tension with water ($\sigma_{Hg\text{-}W,1}$ = 375 dyn/cm and $\sigma_{Hg\text{-}W,2}$ = 415 dyn/cm), Table 2, remain practically constant. Even when the porosity ratio slightly deviates from unity, assuming $\sigma_{Hg\text{-}W,1}$ the Leverett scaling parameter underestimates by 14%, similar to the largest deviations observed in literature, while in the case of $\sigma_{Hg\text{-}W,2}$ the underestimation increases by 26%. In MS1, the agreement with the Leverett scaled values does not improve as the porosity ratio approaches unity but rather worsens, with overestimations ranging from 23.8% to 36.4% with $\sigma_{Hg\text{-}W,1}$, and from 37% to 50.9% with $\sigma_{Hg\text{-}W,2}$. The reason why this deficiency exists when using Leverett scaling in the Hg^0-Water systems analysed is yet to be clarified. Most likely, the fluid properties of liquid mercury play a crucial role, and a microscale evidence of liquid Hg^0 interaction with water within the pores might give further insight into this behaviour.

4.4. Hg^0 infiltration in variably water saturated systems

Based on the required DNAPL heads, the capacity of Hg^0 to infiltrate in partially water saturated porous media is lower than PCE and Hg^0 in fully water saturated systems (Fig. 11; Table 4). The elemental mercury entry head in a partially water saturated system was 5.6% higher than for PCE in fully water saturated conditions for MS1, while it was practically the same of PCE for MS2. For the partially water saturated MS1 sample, Hg^0 required to overcome an entry head 68.9% higher than required in the fully water saturated counterpart. Also for MS2, the entry head in the partially water saturated system was higher than for the fully water saturated counterpart, by 25.8%.

The mercury entry heads were determined at residual water saturations and it could be expected that entry heads would increase further at lower partial water contents. Therefore, assuming Leverett scaling to be applicable (Section 4.2), the Hg^0 entry head at zero water saturation (namely 100% air saturation) was estimated, for both sands, based on the measured Hg^0 and PCE entry heads in water saturated media (Table 4).

By substituting the elemental mercury surface tension (Table 2) in lieu of its interfacial tension with water in Eq. 4, and assuming the Hg^0-Water and PCE-Water systems to be the two respective references for the scaling of the Hg^0-Air retention properties, two different estimates of Hg^0 entry head values can be derived at zero water saturation for both sands (assuming only the value of 375 dyn/cm for $\sigma_{Hg\text{-}w}$, since it was the only one giving a sort of agreement with the experimental evidence when using Leverett scaling, as shown in Section 4.2). This results in two estimated entry head values of fictitious completely dry MS1 and MS2 samples. The Leverett scaled PCE-Water values of the Hg^0 entry head at zero water saturation (Fig. 14) are 16.1% and 22.7% higher than the experimental observations for the partially water saturated samples, for MS1 and MS2, respectively. For the Hg^0-Water scaled values (Fig. 14), only the scaled entry head in MS2 is higher, 2.8%, than for the partially water saturated sample. Conversely, for MS1 the scaled value of the Hg^0 entry head at zero water saturation is 23.4% lower. Nevertheless, in both cases, the scaled values are higher than the measured Hg^0 entry heads for the water saturated conditions, 29.3% for the Hg^0-Water scaled values, and 96% and 54.4% for the PCE-Water scaled values, for MS1 and MS2, respectively. How entry head develops in more detail with decreasing water content remains to be explored. However, considering the spread in the scaled estimates for the entry head at zero water saturation, the entry head in the

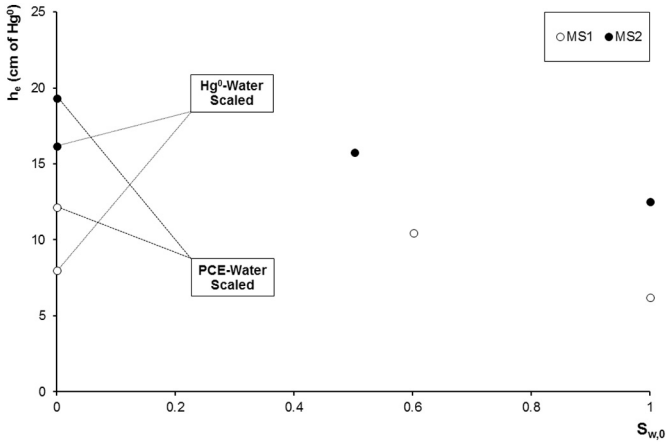

Fig. 14. Hg^0 entry head (h_e) versus initial water saturation ($S_{w,0}$) for MS1 and MS2 (measured and scaled values).

partially water saturated (residual) conditions is possibly already controlled by the larger, air filled pores.

4.5. Experimental scaling parameters for Hg^0-air-water systems

In Table 5, the observed Hg^0-Air-Water scaling parameter (β_{naw}), defined as the ratio (α_{naw}/α_{aw}) between the Hg^0-Air-Water and the Air-Water α parameter, is reported together with the Leverett scaled value (0.148), given as the ratio ($\sigma_{A\text{-}W}/\sigma_{Hg\text{-}A}$) between the water and the DNAPL surface tensions, Table 2, (Lenhard and Parker, 1987), for MS1 and MS2, respectively. In particular, the scaling procedure is limited to the experimental set of MS1c-MS1c_bis and MS2c-MS2c_bis because the respective Air-Water and Hg^0-Air-Water $P_c(S)$ curves were determined on the same porous sample (Section 2.4), and thus on identical pore structure, ideal for an accurate and reliable scaling.

As for the Hg^0-Water system (Section 4.3), there is a poor agreement between experimental and Leverett determinations for the Hg^0-Air-Water system. Even though the pore structure is exactly the same, the experimentally derived scaling parameter is 9.6% higher than the scaled value for MS1, and 28.6% higher for MS2.

The deviations found in both two- and three-phase systems may suggest that the classical scaling theory is less able to cope with Hg^0 retention properties than for other NAPLs. Still, the order of magnitude of the experimental scaling parameters is similar to that of the determinations based solely on the fluids properties, thus not excluding its application to elemental mercury DNAPL. Among the reasons for the observed discrepancies is probably that, if the porous medium is partially water saturated to a degree that allows air to be continuous within the pores, the Hg^0 that tries to infiltrate is expected to be predominantly in contact with air. However, as the sample is water wet, it is also in contact with water, hence the Leverett scaling parameter, defined as the ratio of water and Hg^0 surface tensions, may not be accurate and the effect induced by the Hg^0 interfacial tension with water could be relevant. Since liquid Hg^0 is in contact with both air and water, different contact angles may also arise, thus further influencing its flow behaviour. Furthermore, once infiltration occurs in a partially water saturated porous medium, elemental mercury displaces both air and water (Section 3.2), depending on the initial water distribution within the pores.

5. Conclusions

Liquid elemental mercury shows a deviating infiltration behaviour with respect to more extensively studied DNAPLs, such as PCE. Both theory and experiments confirmed that elemental mercury behaves as a nonwetting fluid requiring to overcome an entry head to infiltrate, not only in fully, but also in partially water saturated porous media.

As for other DNAPLs, the pore structure of the porous medium has an important control on the infiltration behaviour of elemental mercury, as illustrated by the experimental correlation of entry head with intrinsic permeability for the tested glass beads samples. For fully water saturated systems, experimental results showed that Hg^0 DNAPL has a higher capacity to infiltrate than PCE, based on the DNAPL heads required. Although Leverett scaling is able to reproduce the natural tendency of Hg^0 to be more prone than PCE to infiltrate in water saturated porous media, it considerably underestimates this behaviour in comparison with the experimental results.

Most strikingly, and in contrast with other DNAPLs, in partially water saturated systems, the capacity of Hg^0 DNAPL to infiltrate is considerably lower than in fully water saturated systems. Furthermore, once Hg^0 infiltration occurs in a partially water saturated porous medium, experiments showed that elemental mercury displaces both air and water, depending on the initial water distribution within the pores. The results indicate that the conventional wettability hierarchy, in which the NAPL has an intermediate wetting state between the air and the water phases, is not valid for liquid elemental mercury. Therefore, especially for future modelling, a new formulation of the constitutive relations governing elemental mercury DNAPL infiltration and flow behaviour in variably water saturated porous media is required.

Acknowledgements

This research was financially supported by the P.O.R. Campania FSE 2007/2013-2014/2020.

Appendix A. Appendix

A.1. The Graphical Method

In the graphical method (Sillers et al., 2001; Pasha et al. 2015) the nonwetting phase entry head is obtained as the intersection of two straight lines (Fig. A.1): the first line, vertical and asymptotic to the $P_c(S)$ data at zero capillary head, is representative of the zone prior to the nonwetting phase infiltration, while the second line, tangent to the inflection point and obtained by fitting the central branch of the $P_c(S)$ data, is representative of the zone when the nonwetting phase becomes connected within the pores.

Table 5
Hg^0-Air-Water Scaling Parameter (β_{naw}).

Sample	Leverett ($\sigma_{A\text{-}W}/\sigma_{Hg\text{-}A}$)	Experimental (α_{naw}/α_{aw})
MS1c_bis	0.148	0.163
MS2c_bis	0.148	0.191

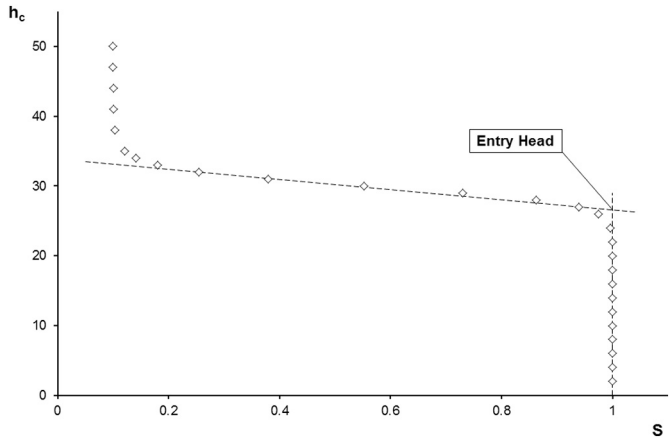

Fig. A.1. Illustration of the graphical method. Measured data (symbols) and intersecting lines (dashed lines).

A.2. Nonwetting Phase Entry Heads Estimation: Methods Comparison

The nonwetting phase entry heads were estimated in different ways, namely with the graphical method (Sillers et al., 2001; Pasha et al. 2015), the α van Genuchten parameter, as $h_e = 1/\alpha$, and the Brooks-Corey model (Brooks and Corey, 1964). The results provided by the three methods are shown in Table A.1.

Table A.1
Nonwetting phase entry heads estimation with different methods.

Sample	System	h_e (cm of water)			h_e (cm of NAPL)		
		Graphical method	1/α	Brooks-corey	Graphical method	1/α	Brooks-corey
Coarse GB	Hg^0-Water	38.40	59.90	44.01	2.84	4.43	3.25
Medium GB	Hg^0-Water	113.03	140.70	105.60	8.36	10.40	7.81
Fine GB	Hg^0-Water	262.71	311.63	245.43	19.42	23.04	18.15
MS1a	Air-Water	24.02	27.17	24.12	–	–	–
MS1b	Air-Water	25.13	28.69	24.83	–	–	–
MS1c	Air-Water	26.10	29.93	26.08	–	–	–
MS2a	Air-Water	39.58	44.79	38.47	–	–	–
MS2b	Air-Water	40.04	44.88	39.95	–	–	–
MS2c	Air-Water	40.32	44.83	40.43	–	–	–
MS1d	PCE-Water	16.17	19.33	15.86	9.90	11.84	9.71
MS2d	PCE-Water	25.75	27.41	24.67	15.77	16.79	15.11
MS1e	Hg^0-Water	83.69	114.31	86.78	6.19	8.45	6.42
MS2e	Hg^0-Water	169.19	204.60	172.09	12.51	15.13	12.72
MS1c_bis	Hg^0-Air-Water	141.33	184.04	137.66	10.45	13.61	10.18
MS2c_bis	Hg^0-Air-Water	212.90	234.76	211.30	15.74	17.36	15.62

The comparison among the entry heads given by the three methods indicates that the van Genuchten fit leads to substantial overestimations of the entry head with respect to the graphical method. This is in agreement with the literature, as it has been shown that 1/α is only relatively related to the entry head (van Genuchten and Nielsen, 1985). Therefore, the 1/α value was not taken into account as an indication of the entry head. The Brooks-Corey model, which actually incorporates the entry head in its formulation, gives values more similar to those obtained by the graphical method. However, since the van Genuchten-Mualem model (Mualem, 1976; van Genuchten, 1980) was chosen to fit the $P_c(S)$ curves (Section 2.4), the graphical method was chosen to determine the nonwetting phase entry heads.

References

Adamson, A.W., Gast, A.P., 1997. Physical Chemistry of Surfaces, 6 Ed. Wiley.

Arbestain, M.C., Rodriguez-Lado, L., Bao, M., Macias, F., 2009. Assessment of mercury-polluted soils adjacent to an old mercury-fulminate production plant. Appl. Environ. Soil Sci. 2009, 1–8. http://dx.doi.org/10.1155/2009/387419.

Bear, J., 1972. Dynamics of Fluids in Porous Media. Dover Publications, Inc., New York.

Bernaus, A., Gaona, X., van Ree, D., Valiente, M., 2006. Determination of mercury in polluted soils surrounding a chlor-alkali plant: direct speciation by X-ray absorption spectroscopy techniques and preliminary geochemical characterisation of the area. Anal. Chim. Acta 565 (1), 73–80.

Biester, H., Müller, G., Schöler, H.F., 2002. Estimating distribution and retention of mercury in three different soils contaminated by emissions from chlor-alkali plants: part I. Sci. Total Environ. 284 (1), 177–189.

Bollen, A., Wenke, A., Biester, H., 2008. Mercury speciation analyses in $HgCl_2$-contaminated soils and groundwater - implications for risk assessment and remediation strategies. Water Res. 42 (1), 91–100.

Brooks, R.H., Corey, A.T., 1964. Hydraulic properties of porous media and their relation to drainage design. Transac. ASAE 7 (1), 26–0028.

Brooks, S.C., Southworth, G.R., 2011. History of mercury use and environmental contamination at the Oak Ridge Y-12 Plant. Environ. Pollut. 159 (1), 219–228.

Busby, R.D., Lenhard, R.J., Rolston, D.E., 1995. An investigation of saturation-capillary pressure relations in two-and three-fluid Systems for Several NAPLS in different porous media. Ground Water 33 (4), 570–578.

CRC, 2014. Handbook of Chemistry and Physics, 94th ed. (Internet Version 2014).

D'Aniello, A., 2017. The Flow Behaviour of Elemental Mercury DNAPL in Porous Media. PhD Thesis. Università degli Studi di Napoli Federico II.

D'Aniello, A., Hartog, N., Sweijen, T., Pianese, D., 2018. Infiltration and distribution of

elemental mercury DNAPL in water-saturated porous media: experimental and numerical investigation. Water Air Soil Pollut. http://dx.doi.org/10.1007/s11270-017-3674-0.
Davis, A., Bloom, N.S., Que Hee, S.S., 1997. The environmental geochemistry and bioaccessibility of mercury in soils and sediments: a review. Risk Anal. 17 (5), 557–569.
Deeb, R., Hawley, E., Kell, L., O'Laskey, R., 2011. Assessing Alternative Endpoints for Groundwater Remediation at Contaminated Sites. (ESTCP-Project ER-200832).
Demond, A.H., Roberts, P.V., 1991. Effect of interfacial forces on two-phase capillary pressure-saturation relationships. Water Resour. Res. 27 (3), 423–437.
Devasena, M., Nambi, I.M., 2010. Migration and entrapment of mercury in porous media. J. Contam. Hydrol. 117, 60–70.
Eichholz, G.G., Petelka, M.F., Kury, R.L., 1988. Migration of elemental mercury through soil from simulated burial sites. Water Res. 22 (1), 15–20.
FILCOM, 2015. Technical Datasheet Filtersand 0.2-0.5 mm and Silversand S60.
Golder Associates, 2011. 2010 Conceptual Site Model - Botany. Report No. 107623162_001_R_Rev0.
González-Fernández, B., Menéndez-Casares, E., Meléndez-Asensio, M., Fernández-Menéndez, S., Ramos-Muñiz, F., Cruz-Hernández, P., González-Quirós, A., 2014. Sources of mercury in groundwater and soils of west Gijón (Asturias, NW Spain). Sci. Total Environ. 481, 217–231.
Hecht, Glaswarenfabrik Karl, 2013. Technical Datasheet 1 mm Glass Beads.
Hofstee, C., Dane, J.H., Walker, R.C., 1998a. Infiltration and redistribution of perchloroethylene in stratified water-saturated porous media. Soil Sci. Soc. Am. J. 62 (1), 13–22.
Hofstee, C., Oostrom, M., Dane, J.H., Walker, R.C., 1998b. Infiltration and redistribution of perchloroethylene in partially saturated, stratified porous media. J. Contam. Hydrol. 34 (4), 293–313.
Hylander, L.D., Meili, M., 2003. 500 years of mercury production: global annual inventory by region until 2000 and associated emissions. Sci. Total Environ. 304 (1), 13–27.
Imhoff, P.T., Gleyzer, S.N., McBride, J.F., Vancho, L.A., Okuda, I., Miller, C.T., 1995. Cosolvent-enhanced remediation of residual dense nonaqueous phase liquids: experimental investigation. Environ. Sci. Technol. 29 (8), 1966–1976.
ITRC, 2012. Using Remediation Risk Management to Address Groundwater Cleanup Challenges at Complex Sites. pp. 31.
Lechler, P.J., Miller, J.R., Lacerda, L.D., Vinson, D., Bonzongo, J.C., Lyons, W.B., Warwick, J.J., 2000. Elevated mercury concentrations in soils, sediments, water, and fish of the Madeira River basin, Brazilian Amazon: a function of natural enrichments? Sci. Total Environ. 260 (1), 87–96.
Lenhard, R.J., Parker, J.C., 1987. Measurement and prediction of saturation-pressure relationships in three-phase porous media systems. J. Contam. Hydrol. 1, 407–424.
Leterme, B., Jacques, D., 2013. Literature Review on Mercury Speciation Soil Systems Under Oxidizing Conditions. Snowman Network. (IMaHG Report, Project No. SN-03/08).
Leterme, B., Blanc, P., Jacques, D., 2014. A reactive transport model for mercury fate in soil-application to different anthropogenic pollution sources. Environ. Sci. Pollut. Res. 21 (21), 12279–12293.
Leverett, M., 1941. Capillary behavior in porous solids. Transactions of the AIME 142 (01), 152–169.
Mayer, A., Hassanizadeh, S.M., 2005. Soil and Groundwater Contamination: Nonaqueous Phase Liquids, Principles and Observations. American Geophysical Union.
Mercer, J.W., Cohen, R.M., 1990. A review of immiscible fluids in the subsurface: properties, models, characterization and remediation. J. Contam. Hydrol. 6 (2), 107–163.
Miller, C.L., Watson, D.B., Lester, B.P., Lowe, K.A., Pierce, E.M., Liang, L., 2013. Characterization of soils from an industrial complex contaminated with elemental mercury. Environ. Res. 125, 20–29.
Mualem, Y., 1976. A new model for predicting the hydraulic conductivity of unsaturated porous media. Water Resour. Res. 12 (3), 513–522.
Newsham, K.E., Rushing, J.A., Lasswell, P.M., Cox, J.C., Blasingame, T.A., 2004. A Comparative Study of Laboratory Techniques for Measuring Capillary Pressures in Tight Gas Sands. In SPE Annual Technical Conference and Exhibition, Society of Petroleum Engineers.
Oostrom, M., Hofstee, C., Walker, R.C., Dane, J.H., 1999. Movement and remediation of trichloroethylene in a saturated heterogeneous porous medium: 1. Spill behavior and initial dissolution. J. Contam. Hydrol. 37 (1), 159–178.
Oostrom, M., Hofstee, C., Lenhard, R.J., Wietsma, T.W., 2003. Flow behavior and residual saturation formation of liquid carbon tetrachloride in unsaturated heterogeneous porous media. J. Contam. Hydrol. 64 (1), 93–112.
Parker, J.C., Lenhard, R.J., Kuppusamy, T., 1987. A parametric model for constitutive properties governing multiphase flow in porous media. Water Resour. Res. 23 (4), 618–624.
Pasha, A.Y., Khoshghalb, A., Khalili, N., 2015. Pitfalls in interpretation of gravimetric water content-based soil-water characteristic curve for deformable porous media. Int. J. Geomech. 16 (6), D4015004.
Pennell, K.D., Pope, G.A., Abriola, L.M., 1996. Influence of viscous and buoyancy forces on the mobilization of residual tetrachloroethylene during surfactant flushing. Environ. Sci. Technol. 30 (4), 1328–1335.
Pittman, E.D., 1992. Relationship of porosity and permeability to various parameters derived from mercury injection-capillary pressure curves for sandstone. Am. Assoc. Pet. Geol. Bull. 76 (2), 191–198.
Retsch, 2013. Technical Datasheet 0.10–0.25 mm and 0.20–0.50 mm Glass Beads.
Risher, J.F., 2003. Elemental mercury and inorganic mercury compounds: human health aspects. Concise International Chemical Assessment Document. World Health Organization, Geneva.
Ruth, D., Lindsay, C., Allen, M., 2013. Combining electrical measurements and mercury porosimetry to predict permeability. Petrophysics 54 (06), 531–537.
Scanlon, B.R., Tachovsky, J.A., Reedy, R., Nicot, J.P., Keese, K., Slade, R.M., Merwad, V., Howard, M.T., Wells, G.L., Mullins, G.J., Ortiz, D.M., 2005. Groundwater–surface water interactions in Texas. In: Implications for Water Resources and Contaminant Transport (TCEQ). Bureau of Economic Geology, The University of Texas at Austin, pp. 129–131.
Schwille, F., 1988. Dense Chlorinated Solvents in Porous and Fractured Media - Model Experiments. Lewis Publishers, Chelsea, MI.
Seki, K., 2007. SWRC fit - a nonlinear fitting program with a water retention curve for soils having unimodal and bimodal pore structure. Hydrol. Earth Syst. Sci. Discuss. 4, 407–437.
Sillers, W.S., Fredlund, D.G., Zakerzadeh, N., 2001. Mathematical attributes of some soil-water characteristic curve models. In: In Unsaturated Soil Concepts and Their Application in Geotechnical Practice. Springer, Netherlands, pp. 243–283.
Smith, J.D., Chatzis, I., Ioannidis, M.A., 2002. A new technique for measuring the breakthrough capillary pressure. Soc. Core Anal. 40, 2002.
Sweijen, T., Hartog, N., Marsman, A., Keijzer, T.J., 2014. The transport behaviour of elemental mercury DNAPL in saturated porous media: analysis of field observations and two-phase flow modelling. J. Contam. Hydrol. 161, 24–34.
UNEP, 2002. Global Mercury Assessment. Switzerland, Geneva.
US DOE, 2001. Mercury Contaminated Material Decontamination Methods: Investigation and Assessment. (DE-FG21-95EW55094).
US EPA, 2007a. Treatment Technologies for Mercury in Soil, Waste, and Water. EPA Report 542-R-07-003 US Environmental Protection Agency, Office of Superfund Remediation and Technology Innovation.
US EPA, 2007b. Elemental Mercury. (EPA Archive Document, www.epa.gov/mercury).
van Genuchten, M.T., 1980. A closed form equation for predicting the hydraulic conductivity of unsaturated soils. Soil Sci. Soc. Am. J. 44, 892–898.
van Genuchten, M.T., Nielsen, D.R., 1985. On describing and predicting the hydraulic properties of unsaturated soils. Ann. Geophys. 3 (5), 615–628.
Vavra, C.L., Kaldi, J.G., Sneider, R.M., 1992. Geological applications of capillary pressure: a review. Am. Assoc. Pet. Geol. Bull. 76 (6), 840–850.
Walvoord, M.A., Andraski, B.J., Krabbenhoft, D.P., Striegl, R.G., 2008. Transport of elemental mercury in the unsaturated zone from a waste disposal site in an arid region. Appl. Geochem. 23 (3), 572–583.
Wardlaw, N.C., Taylor, R.P., 1976. Mercury capillary pressure curves and the intepretation of pore structure and capillary behaviour in reservoir rocks. Bull. Can. Petrol. Geol. 24 (2), 225–262.
Wentworth, C.K., 1922. A scale of grade and class terms for clastic sediments. J. Geol. 30 (5), 377–392.
White, M.D., Oostrom, M., Lenhard, R.J., 2004. A practical model for mobile, residual, and entrapped NAPL in water-wet porous media. Ground Water 42 (5), 734–746.
World Chlorine Council, 2011. Reduction of mercury emissions and use from the chlor-alkali sector partnership.
Wu, W.J., Delshad, M., Oolman, T., Pope, G.A., 2000. Remedial options for creosote-contaminated sites. Groundwater Monitoring & Remediation 20 (2), 78–86.

Notation

Greek symbols

α: van Genuchten model parameter
α_{naw}/α_{aw}: ratio between Hg^0-Air-Water and Air-Water α parameters
α_{nw}/α_{aw}: ratio between DNAPL-Water and Air-Water α parameters
β_{naw}: Hg^0-Air-Water system scaling parameter
β_{nw}: DNAPL-Water system scaling parameter
ρ_{Hg}: elemental mercury density
ρ_{PCE}: tetrachloroethylene density
ρ_s: particle density
$\sigma_{A\text{-}W}$: water surface tension
$\sigma_{Hg\text{-}A}$: elemental mercury surface tension
$\sigma_{Hg\text{-}W}$: interfacial tension between elemental mercury and water
$\sigma_{PCE\text{-}W}$: interfacial tension between tetrachloroethylene and water
ϕ: porosity
ϕ_{nw}/ϕ_{aw}: ratio between DNAPL-Water and Air-Water samples porosity

Latin symbols

d_{50}: median particle diameter
h_{aw}: capillary head between air and water
h_c: capillary head
h_e: nonwetting phase entry head
h_n: NAPL head
h_{nw}: capillary head between NAPL and water
J: Leverett function
k_{max}: intrinsic permeability, maximum measured value
k_{mean}: intrinsic permeability, arithmetic mean value
k_{min}: intrinsic permeability, minimum measured value
n: van Genuchten model parameter
P_c: capillary pressure
S: wetting phase saturation
$\bar{S}$: effective wetting phase saturation
Sn: NAPL saturation
S_t: total liquid saturation
S_w: water saturation
$S_{w,ir}$: irreducible water saturation
$S_{w,o}$: initial water saturation